DOI: 10.1002/ange.201209473

Fe^{II}/Fe^{III} Charge Order

$Sr_4Fe_6O_{12}$: Low-Temperature Fe^{2+}–Fe^{3+} Charge Order within Pairs of Edge-Linked Tetrahedra**

*Min Feng Lü, João C. Waerenborgh, and Colin Greaves**

Charge order (CO; where a delocalized mixed-valent state, e.g. $Fe^{2.5+}$, orders on cooling to give charge localization with different charges, e.g. Fe^{2+} and Fe^{3+}, on different sites) or charge disproportion in mixed-valence transition-metal oxides provides the basis for important electronic and magnetic properties, for example:

- stripes of varying charge have been linked to the mechanism of high-temperature superconductivity in copper oxides;[1]
- charge order, coupled with orbital and magnetic ordering has also been linked with Colossal Magnetoresistance[2] and multiferroic properties[3] in mixed-valence manganites;
- Fe^{2+}–Fe^{3+} charge order drives the Verwey transition at 120 K in Fe_3O_4,[4] the details of which still attract interest.[5]

Charge order generally occurs in compounds containing five-coordinate or six-coordinate transition-metal cations, and we are unaware of any examples that relate to tetrahedral coordination of d-block transition metals—the relative change in bond lengths to accommodate the different cation charges increases as the coordination number decreases, which enhances structural strain. Herein, we describe the use of low-temperature topochemical hydride reduction methods to obtain the first reported structure containing an extended array of linked pairs of edge-sharing FeO_4 tetrahedra; charge order occurs within the tetrahedra at low temperatures.

The layered perovskite-like phases with composition $Sr_4Fe_6O_{13\pm\delta}$ have alternating layers of six- and five-coordinate Fe,[6] and can display high mixed (ionic and electronic) conductivity. They therefore have important potential for electrodes in solid-oxide fuel cells, and have been subject to significant fundamental investigation.[7] The species with the lowest oxygen content has been assumed to have the composition $Sr_4Fe_6O_{12}$, with an average oxidation state of $Fe^{2.667+}$ ($4\,Fe^{3+}$ and $2\,Fe^{2+}$). However, this composition has never been prepared although its structure has been predicted: octahedral Fe^{3+} layers separated by layers of square pyramidal $Fe^{2.5+}O_5$ units, Figure 1.[8] Recently, the use of low-temperature hydride reduction has achieved notable success in obtaining transition-metal ions in low oxidation states and unusual coordination. Of particular significance has been the successful synthesis of perovskite-related "infinite layer" compounds, with layers of infinitely repeating square MO_2 units, where M = Fe, Co, Ni,[9] and three-coordinate Fe^{2+} ions in an $n=3$ Ruddlesden–Popper phase.[10] In contrast to previous unsuccessful high-temperature synthesis attempts,[11,12] herein we report the low-temperature synthesis of $Sr_4Fe_6O_{12}$; we describe its unique structure and unusual charge order properties.

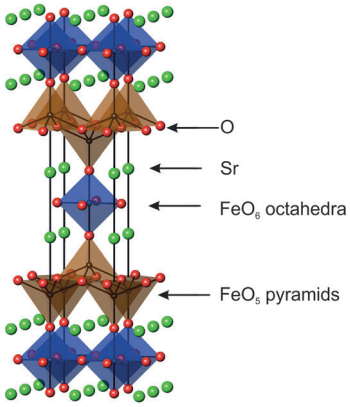

Figure 1. Predicted structure of $Sr_4Fe_6O_{12}$.[8]

X-ray powder diffraction (XRD) confirmed the orthorhombic symmetry for precursor samples of $Sr_4Fe_6O_{13\pm\delta}$.[11,12] Reduction using CaH_2 yielded a primitive tetragonal phase (Supporting Information: synchrotron XRD data, Figure S1; electron-diffraction patterns, Figure S2) with $a=5.5413(2)$ Å, $c=19.3736(9)$ Å, larger than predicted.[8] Although the high XRD resolution indicated possible space groups, full analysis was prevented by severe texture effects and the low oxygen scattering factor. Energy dispersive spectroscopy confirmed that the ratio Sr:Fe = 4:6 after reduction, and thermal analysis (Figure S3) showed the material to be air-sensitive.

Magnetic susceptibility data (Figure S4) indicated that $Sr_4Fe_6O_{12}$ is a canted antiferromagnet with $T_N > 300$ K. The

[*] Dr. M. F. Lü
State Key Laboratory of Rare Earth Resource Utilization
Changchun Institute of Applied Chemistry, CAS
Changchun (PR China)
Dr. J. C. Waerenborgh
IST/ITN, Instituto Superior Técnico, Universidade Técnica de Lisboa
CFMC-UL, 2686-953, Sacavém (Portugal)
Prof. C. Greaves
School of Chemistry, University of Birmingham
Birmingham B15 2TT (UK)
E-mail: c.greaves@bham.ac.uk

[**] We are grateful to EPSRC for the provision of NPD facilities, and to Dr. Pascal Manuel for advice and technical assistance. We also acknowledge assistance from Tie Ying Yang for the collection of synchrotron data. Financial support from FCT (PTDC/CTM-CER/114561/2009), Portugal and National Natural Science Foundation of China (Grant No. 20771100) is gratefully acknowledged.

Supporting information for this article is available on the WWW under http://dx.doi.org/10.1002/anie.201209473.

ferromagnetic component at 5 K (Figure S5) is approximately 0.1 μ_B per Fe. The variation in susceptibility at approximately 120 K suggested a possible structural/electronic transition, and a detailed variable temperature time-of-flight (TOF) neutron powder diffraction (NPD) study was conducted to determine the structure and its temperature dependence.

The NPD data revealed that $Sr_4Fe_6O_{12}$ was unstable at temperatures ($T > 600$ K) approaching the Néel temperature T_N, so structure analysis focused on the range 300–5 K, where the presence of magnetic scattering hindered structure determination. Although preliminary XRD data had confirmed the cation arrangement shown in Figure 1, the NPD data revealed that the oxygen framework was very different with respect to the O atoms within the square-pyramidal region of Figure 1. Space group $P4_2$ provided a chemically sensible model with tetrahedrally coordinated Fe atoms between the octahedral layers, but the refinement was unstable; the poor agreement in the low Q profile region suggested a major problem related to the neglect of magnetic scattering.

Knowledge of the basic structure, comprising bilayers of tetrahedra separated by monolayers of octahedra, allowed evaluation of the basic magnetic order (see below). An iterative process resulted in additional symmetry elements becoming apparent, and the final refinement was performed in space group $P4_2/mnm$, ($a = 5.425(3)$ Å, $c = 19.383(2)$ Å), consistent with XRD data; structural parameters are given in the Supporting Information, Table S1 and bond lengths and angles for the Fe polyhedra in Table 1. These data were

Table 1: Fe polyhedra bond lengths and angles at 300 K.

Bond lengths [Å]		Bond valence sum	Bond angles [Å]	
Fe1–O1	1.930(3)	2.94(1)	O1-Fe1-O2	90.9(2) [×2]
Fe1–O2	1.9598(1) [×2]		O1-Fe1-O3	180.0(0)
Fe1–O3	1.989(5)		O2-Fe1-O2	178.3(3)
Fe1–O4	2.198(4) [×2]		O2-Fe1-O3	89.1(2) [×2]
Fe2–O4	1.822(4)	2.53(2)	O4-Fe2-O5	109.2(2) [×2]
Fe2–O5	2.029(3) [×2]		O4-Fe2-O5	128.5(2)
Fe2–O5	1.885(5)		O5-Fe2-O5	86.1(3)
			O5-Fe2-O5	107.8(2) [× 2]

obtained using the higher resolution histogram from detector Bank 5 (see Experimental Section), and the NPD profiles from the final refinement are shown in Figure S6. Bond valence sums[13] for the two Fe species (using the Fe^{3+} parameter), Table 1, clearly confirm that octahedral Fe1 is Fe^{3+}, whereas Fe2 consists of an equal proportion of Fe^{2+} and Fe^{3+}. The structure is shown in Figure 2a and the arrangement of the tetrahedral units in the Fe2 regions is shown in Figure 2b and c.

The structure is probably best described as perovskite layers of octahedral Fe1O_6 units separated by two rock-salt-related Fe2O layers. The structure is related to some copper-containing superconductors, and can be compared with $Bi_2Sr_2CuO_6$.[14] In this way, $Sr_4Fe_6O_{12}$ may be written $Fe2_2Sr_2Fe1O_6$, with Fe2 substituted for Bi and Fe1 for Cu.

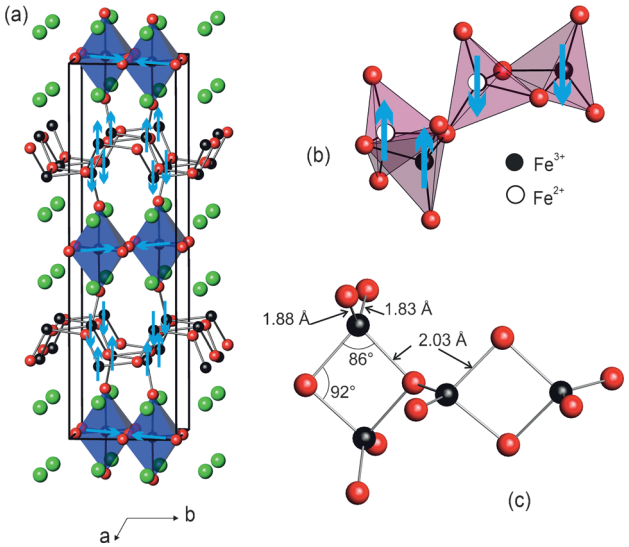

Figure 2. Structure of $Sr_4Fe_6O_{12}$ showing magnetic moment order as light blue arrows: a) full structure highlighting Fe1O_6 octahedra (blue) and Fe2O_4 tetrahedra (bonds); b) arrangement of Fe2 tetrahedra with charge order in adjacent layers at $z \approx 0.3$ (Fe2 atoms on right) and $z \approx 0.2$ (Fe2 atoms on left) along the *c*-axis; c) Fe2 tetrahedra linking viewed approximately down [001] showing bond lengths and angles. Fe black, Sr green, and O red.

For $Sr_4Fe_6O_{12}$, the structural arrangement within the Fe2O layers is more straightforward than for the BiO layers in $Bi_2Sr_2CuO_6$, since structural effects attributed to Bi^{3+} lone-pair electrons are absent. Simple distortions occur to form pairs of Fe2O_4 tetrahedra (Figure S7) that fully satisfy the bonding requirements of $Fe^{2.5+}$. However, the structure contains the highly unusual, and stability restricting, feature of edge-linked tetrahedra. We are aware of only one other structural family with such a feature—$K_6Fe_2O_6$ with isolated pairs of tetrahedra.[15] In $Sr_4Fe_6O_{12}$, it is possible that weak Fe–Fe bonding across the common tetrahedral edge (the Fe2–Fe2 distance is 2.92 Å at 300 K) offers stabilization to compensate the Fe–Fe electrostatic repulsions.

Figure 2 shows that the direction of the edge-linking of the pairs of Fe2O_4 tetrahedra is mutually perpendicular in the two layers of a given bilayer. The tetrahedra are distorted (Figure 2c) because of the high cation repulsions: the two Fe–O bridging distances are respectively 0.14 Å and 0.20 Å longer than the other two bonds, and the bridging O-Fe-O angle is reduced to 86° to minimize repulsion effects. On cooling, changes in unit-cell dimensions (Figure 3) suggested an electronic transition between 160 K and 100 K. Only a very small contraction (0.03%) occurs below 100 K, so some structural consequences of the main charge-order transition may continue at lower temperatures. Energy minimization supports a ground state in which each tetrahedral pair contains one Fe^{2+} and one Fe^{3+} ion, and cooling from 160 K to 100 K results in a small decrease in the Fe2–Fe2 distance (Figure 4), which is compatible with Fe^{2+}–Fe^{3+} rather than $Fe^{2.5+}$–$Fe^{2.5+}$ interactions. No evidence for long-range order between the pairs was apparent. The O5 atoms that bridge the tetrahedral Fe2 ions have high isotropic displacement parameters (IDPs) at both 300 K and 5 K, $U_{iso} = 0.039$ and 0.034 Å^2,

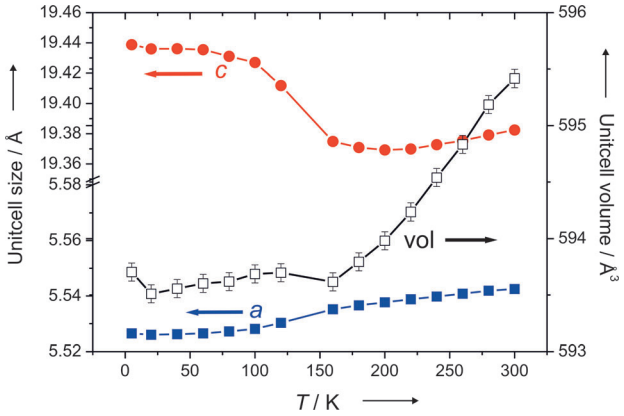

Figure 3. Variation of unit cell dimensions and volume with temperature.

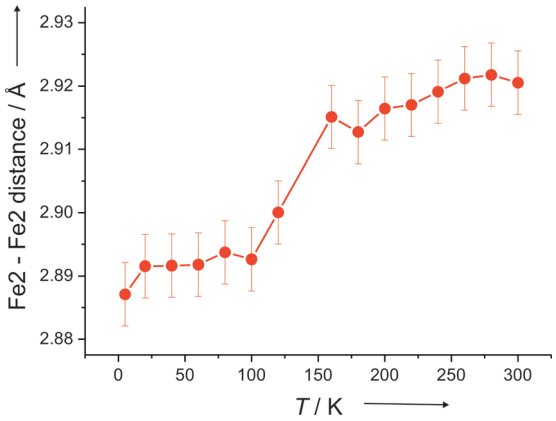

Figure 4. Variation of Fe2–Fe2 distance with temperature.

respectively (Table S1), whereas for a fully delocalized $Fe^{2.5+}$ arrangement, we would expect a unique position for O5 with a normal IDP; even at 300 K, a small degree of charge separation over the Fe2 sites may exist.

Mössbauer spectra were recorded between 295 K and 4 K. At 295 K, the spectrum can be fitted to two sextets which are indicative of octahedral Fe^{3+} and tetrahedral $Fe^{2.5+}$[7,16] (Figure 5, Table S2). At 4 K the sextet for the octahedral Fe^{3+} ion is still observed whereas the signal for the tetrahedral

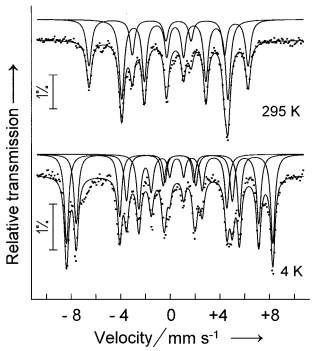

Figure 5. Mössbauer spectra at 295 K and 4 K.

$Fe^{2.5+}$ ion is clearly replaced by two sextets typical of tetrahedrally coordinated Fe^{2+} and Fe^{3+}, respectively. These sextets confirm charge order. Relevant Mössbauer parameters are presented in Table S2.

The spectra at intermediate temperatures (Figure S8), and fitting parameters (Table S2) reveal that the major changes that reflect the onset of charge order occur between 160 K and 80 K, in excellent agreement with the structural changes observed in the NPD data.

The magnetic order was modeled using NPD data obtained at 300 K and 5 K. The final refined magnetic order is shown by the arrows in Figure 2, and the moments are given in Table S3. Each layer of tetrahedral Fe2 has ferromagnetic moments along [001], and these moments are anti-parallel to those in the contiguous layer of Fe2. The Fe1 in the octahedral layers are magnetically frustrated, since their preferred antiferromagnetic order is not compatible with the ferromagnetic order in the adjacent layers. The main magnetic signature within the octahedral layers is antiferromagnetic order with moments aligned along the [110] direction. However, there is an additional small ferromagnetic component along [001], which is aligned antiparallel to the moments in adjacent layers. The ferromagnetic exchange within a pair of edge-linked Fe2 tetrahedra is consistent with direct *e* orbital overlap between Fe^{2+} ($e^3\,t_2^3$) and Fe^{3+} ($e^2\,t_2^3$) centers. The refined magnetic moments (Table S3), suggest that T_N is significantly higher than 300 K. At 5 K, the moment for the tetrahedral Fe2 center is 3.42 μ_B, which is lower than the ideal value of 4.5 μ_B (for mixed Fe^{2+} and Fe^{3+}) indicating a high level of covalence. The moment for Fe1 (2.86 μ_B) is substantially lower than the expected 5.0 μ_B for Fe^{3+}. The NPD data at 5 K (Figure S9) clearly show additional magnetic scattering for 4.2 Å $< d <$ 5.2 Å, and this region was excluded for the final refinements. The additional peaks could be indexed on a supercell ($2a, b, 2c$), but to obtain full details of the magnetic order, single-crystal data will be needed. However, the low moment for the octahedral Fe1 suggests that it may arise from a magnetic modulation centered on this site.

In summary, we describe the synthesis of $Sr_4Fe_6O_{12}$, the parent phase for the widely studied materials $Sr_4Fe_6O_{13\pm\delta}$. The synthesis, involving topotactic reduction, produces a structure that appears unique in having pairs of edge-linked $Fe^{2.5+}O_4$ tetrahedra at 300 K. On cooling, electrostatically driven localized charge order occurs to give one Fe^{3+} and one Fe^{2+} ion within each pair in a localized fashion. This is the first observation of charge order of this type, involving localized order on tetrahedral units, and occurs gradually between 160 K and 80 K, in contrast to the three-dimensional, first order transitions observed in six-coordinate (Fe_3O_4)[4] and five-coordinate ($LnBaFe_2O_5$; Ln = lanthanide)[16b] systems.

Experimental Section

Precursor samples of $Sr_4Fe_6O_{13\pm\delta}$ were prepared by a standard solid-state synthesis.[11] Reduction to $Sr_4Fe_6O_{12}$ was performed using excess CaH_2 as reducing agent in an evacuated pyrex tube heated for 7 days at 493 K.

NPD data were collected on the diffractometer Wish at ISIS, Rutherford Appleton Laboratory, UK. In this study, detector banks

centered at 2θ values of 90° (Bank 3) and the higher resolution 152.9° (Bank 5) were used. 2 g of sample were loaded into a 6 mm diameter vanadium can in a helium glove box, and data were analyzed using GSAS[17] with the EXPGUI interface.[18]

Mössbauer spectra were collected between 295 and 4 K in transmission mode using a conventional constant-acceleration spectrometer and a 25 mCi ^{57}Co source in a Rh matrix. The velocity scale was calibrated using α-Fe foil.

Full synthesis and characterization details are provided as Supporting Information.

Received: November 27, 2012
Revised: February 12, 2013
Published online: March 26, 2013

Keywords: charge order · iron · layered compounds · neutron diffraction · solid-state structures

[1] M. I. Salkola, V. J. Emery, S. A. Kivelson, *Phys. Rev. Lett.* **1996**, *77*, 155 – 158.
[2] a) H. Yoshizawa, H. Kawano, Y. Tomioka, Y. Tokura, *Phys. Rev. B* **1995**, *52*, R13145 – R13148; b) P. G. Radaelli, D. E. Cox, M. Marezio, S.-W. Cheong, *Phys. Rev. B* **1997**, *55*, 3015 – 3023.
[3] a) D. V. Efremov, J. V. D. Brink, D. I. Khomskii, *Nat. Mater.* **2004**, *3*, 853 – 856; b) S. Mercone, A. Wahl, A. Pautrat, M. Pollet, C. Simon, *Phys. Rev. B* **2004**, *69*, 174433.
[4] E. J. W. Verwey, *Nature* **1939**, *144*, 327 – 328.
[5] M. S. Senn, J. P. Wright, J. P. Attfield, *Nature* **2012**, *481*, 173 – 176.
[6] a) F. Kanamaru, M. Shimada, M. Kiozumi, *J. Phys. Chem. Solids* **1972**, *33*, 1169 – 1171; b) A. Yoshiasa, K. Ueno, F. Kanamaru, H. Horiuchi, *Mater. Res. Bull.* **1986**, *21*, 175 – 181.
[7] J. C. Waerenborgh, M. Avdeev, M. V. Patrakeev, V. V. Kharton, J. R. Frade, *Mater. Lett.* **2003**, *57*, 3245 – 3250, and references therein.
[8] B. Raveau, M. Hervieu, D. Pelloquin, C. Michel, R. Retoux, *Z. Anorg. Allg. Chem.* **2005**, *631*, 1831 – 1839.
[9] a) M. A. Hayward, M. A. Green, M. J. Rosseinsky, J. Sloan, *J. Am. Chem. Soc.* **1999**, *121*, 8843 – 8854; b) V. V. Poltavets, K. A. Lokshin, S. Dikmen, M. Croft, T. Egami, M. Greenblatt, *J. Am. Chem. Soc.* **2006**, *128*, 9050 – 9051; c) Y. Tsujimoto, C. Tassel, N. Hayashi, T. Watanabe, H. Hageyama, K. Yoshimura, M. Takano, M. Ceretti, C. Ritter, W. Paulus, *Nature* **2007**, *450*, 1062 – 1065; d) M. A. Hayward, E. J. Cussen, J. B. Claridge, M. Bieringer, M. J. Rosseinsky, C. J. Kiely, S. J. Blundell, I. M. Marshall, F. L. Pratt, *Science* **2002**, *295*, 1882 – 1884.
[10] A. Bowman, M. Alix, D. Pelloquin, M. J. Rosseinsky, *J. Am. Chem. Soc.* **2006**, *128*, 12606 – 12607.
[11] M. Y. Avdeev, M. V. Patrakeev, V. V. Kharton, J. R. Frade, *J. Solid State Electrochem.* **2002**, *6*, 217 – 224.
[12] M. D. Rossell, A. M. Abakumov, G. Van Tendeloo, M. V. Lomakov, S. Y. Istomin, E. V. Antipov, *Chem. Mater.* **2005**, *17*, 4717 – 4726.
[13] I. D. Brown, D. Altermatt, *Acta Crystallogr. Sect. B* **1985**, *41*, 244 – 247.
[14] C. C. Torardi, M. A. Subramanian, J. C. Calabrese, J. Gopalakrishnan, E. M. McCarron, K. J. Morrissey, T. R. Askew, R. B. Flippen, U. Chowdry, A. W. Sleight, *Phys. Rev. B* **1988**, *38*, 225 – 231.
[15] a) H. Rieck, R. Hoppe, *Angew. Chem.* **1973**, *85*, 589; *Angew. Chem. Int. Ed. Engl.* **1973**, *12*, 673; b) G. Frisch, C. Röhr, *Z. Naturforsch. B* **2005**, *60*, 732.
[16] a) J. Lindén, P. Karen, A. Kjekshus, J. Miettinen, T. Pietari, M. Karppinen, *Phys. Rev. B* **1999**, *60*, 15251 – 15260; b) P. Karen, P. M. Woodward, J. Lindén, T. Vogt, A. Studer, P. Fischer, *Phys. Rev. B* **2001**, *64*, 214405; c) J. C. Waerenborgh, D. P. Rojas, N. P. Vyshatko, A. L. Shaula, V. V. Kharton, I. P. Marozau, E. N. Naumovich, *Mater. Lett.* **2003**, *57*, 4388 – 4393.
[17] A. C. Larson, R. B. von Dreele, *General Structure Analysis System (GSAS)* (Los Alamos National Laboratory Report LAUR, 86 – 784, **2000**).
[18] B. H. Toby, *J. Appl. Crystallogr.* **2001**, *34*, 210 – 213.

